Ground movement of shallow buried ellipse cavity in a layered half-space impacted by SH wave

Yuanbo ZHAO, Hui QI

College of Aerospace and Civil Engineering, Harbin Engineering University, Harbin, Heilongjiang 150001, China

Email: ZYB201507@126.com

Abstract: Based on the great arc assumption and the conformal mapping method, the ground surface displacement of shallow buried ellipse hole in a soft layered half-space impacted by SH wave is researched. The great arc assumption is used to simulate the straight boundary and the conformal mapping method is used to deal with the elliptical boundary problems. According to the numerical example, the ground movement amplification coefficient W* is smaller when the layer is harder than the half space and the incident wave number is larger. When the thickness of the layer is fixed, if the layer is softer, the W* is falling off with the down of the ellipse; if the half space if softer, the W* is smallest when the ellipse is in the middle of the layer.

1. Introduction

When the earthquake occurs, the seismic wave propagates to the ground and cause the ground to vibrate, and then cause the building to vibrate and the destruction of the buildings. With the urban development, there are more and more underground projects. It is definitely going to have an impact on the surface movement at the time of the earthquake. The analytic method could give a precise answer to such problems. In 1973, Mow and Pao provided detailed information on the commonly used method for the scattering of elastic waves and dynamic stress concentration [1]. Yuan et al. [2; 3] studied the SH wave scattering problem of a semi-cylindrical hill and the cylindrical hill of circular—arc cross-section. Zhang et al [4] gave the analytical solution to the scattering of cylindrical SH waves by a partially filled semi-circular alluvial valley. In 1982, Liu et al [5] introduced the complex function method which was used for the static problems to solve the scattering dynamic problems of elastic wave and extended the application scope and technique of wave function expansion method. Based on the great arc method, Qi et al [6; 7] researched the Dynamic analysis for the layer half-space with circular cavity and inclusion impacted by SH wave. Zhao [8] and Ding [9] presented the ground surface movement with holes and inclusion impacted by SH wave.

2. Numerical Investigation

2.1. Problem Model and control equantions

The Figure 1 shows the schematic diagram model of the problem researched. As shown in the figure 1, the problem can be described that a single ellipse hole is incased by the upper elastic surface overburden layer of the elastic half-space. Area I is the half-space, area II is the overburden layer. G_i, k_i, and ρ_i respectively express the shear modulus, the wave number and the density of medium. The subscript represents the region. When i=1, it means the region I; when i=2, it means the region II.

T_U and T_D signify upper and lower boundary of the surface layer, respectively. T_E stands for the

boundary of the ellipse hole, whose long axis is a and the short axis is b. Respectively, h_1 and h_2 denote the distance from the center of the ellipse to the upper and lower boundary. The great arc assumption method is used to approximate the upper and lower boundary with infinite radius of arc so that T_U becomes $\widehat{T_U}$ and T_D becomes $\widehat{T_D}$. The ellipse center is defined as the origin of coordinates O_2, and the line parallels to T_U as X_2 axis to establish coordinate system $X_2O_2Y_2$. Meanwhile, Rectangular coordinate system $X_1O_1Y_1$ is established as origin O_2 encased in a layer of elastic half space

$$\begin{cases} h=h_1+h_2 \\ R_U=h+R_D \\ z_2=z_1-i(R_D+h_2) \end{cases} \tag{1}$$

This SH-Wave studied in this paper is the out-of-plane shear movement problem of scattering. The SH-Wave displacement field in the rectangular coordinate system X-Y plane could be indicated as W (X, Y, t),

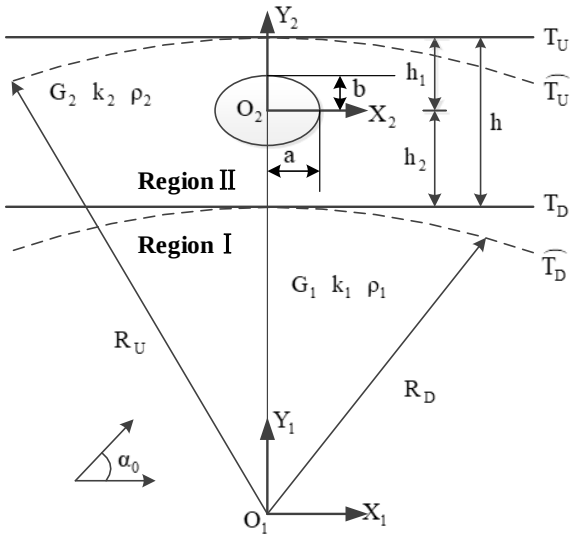

Figure 1 Schematic diagram of the model

which is perpendicular to the X-Y plane. For the steady-state problem, the fields of displacement W(X, Y, t) need to satisfy the following Helmholtz equation：

$$\left(\partial^2 W/\partial X^2\right)+\left(\partial^2 W/\partial Y^2\right)+k^2 W=0 \tag{2}$$

Where $k=\omega/c$, $c^2=G/\rho$, ω is the circular frequency of displacement field W (X, Y, t), G shows the shear modulus of medium, ρ expresses the density of medium. exp(-iωt) means the dependencies of displacement field W (X, Y, t) and time t, and in the following paper, exp(-iωt) is left out because of the problem studied is steady state.

In complex plane, the formula (2) is shown as:

$$4\left(\partial^2 W/\partial z\partial\bar{z}\right)+k^2 W=0 \tag{3}$$

The relationship of stress and strain in the complex plane polar coordinates are:

$$\tau_{Z\rho}=G\left(\frac{\partial W}{\partial z}\frac{z}{|z|}+\frac{\partial W}{\partial \bar{z}}\frac{|z|}{z}\right),\quad \tau_{Z\varphi}=iG\left(\frac{\partial W}{\partial z}\frac{z}{|z|}-\frac{\partial W}{\partial \bar{z}}\frac{|z|}{z}\right) \tag{4}$$

Because of the hole studied in this paper is ellipse, it is very difficult to solve the stress of ellipse hole, the conformal mapping method is need to be used to change the ellipse cavity to circular cavity. The new complex plane is defined as η, and the mapping function is expressed as :

$$z=f(\eta)=p(\eta+q/\eta) \tag{5}$$

In which, $p=(a+b)/2$, $q=(a-b)/(a+b)$, $\eta=r\exp(i\theta)$. a and b respectively represent the long axis and short axis of the ellipse hole.

In the plane η after mapping, the equations (3) and (4) are shown as:

$$4\left(\partial^2 W/\partial\eta\partial\bar{\eta}\right)/f'(\eta)/f'(\bar{\eta})+k^2W=0 \tag{6}$$

$$\tau_{Zr}=\frac{G}{r|f'(\eta)|}\left(\eta\frac{\partial W}{\partial\eta}+\bar{\eta}\frac{\partial W}{\partial\bar{\eta}}\right),\quad \tau_{Z\theta}=\frac{iG}{r|f'(\eta)|}\left(\eta\frac{\partial W}{\partial\eta}-\bar{\eta}\frac{\partial W}{\partial\bar{\eta}}\right) \tag{7}$$

2.2. Wave field and radial stress

The displacement field and radial stress generated by the incident wave in the complex plane z_1 is:

$$W^{(I)}_{(z_1,\bar{z}_1)}=W_0\exp\left[ik_1\mathrm{Re}\left(z_1e^{-i\alpha_0}\right)\right] \tag{8}$$

$$\tau^{(I)}_{z\rho,(z_1,\bar{z}_1)}=\left(ik_1G_1W_0\right)\exp\left[ik_1\mathrm{Re}\left(z_1e^{-i\alpha_0}\right)\right]\mathrm{Re}\left(z_1e^{-i\alpha_0}/|z_1|\right) \tag{9}$$

The displacement field and radial stress generated by the scattering wave $W^{(S1)}$ occurred by T_D in area Ⅰ in the complex plane z_1 is:

$$W^{(S1)}_{(z_1,\bar{z}_1)}=\sum_{n=-\infty}^{n=+\infty}A_nH_n^{(2)}\left(k_1|z_1|\right)\left(z_1/|z_1|\right)^n \tag{10}$$

$$\tau^{(S1)}_{z\rho,(z_1,\bar{z}_1)}=0.5k_1G_1\sum_{n=-\infty}^{n=+\infty}A_n\left[H_{n-1}^{(2)}\left(k_1|z_1|\right)-H_{n+1}^{(2)}\left(k_1|z_1|\right)\right]\left(z_1/|z_1|\right)^n \tag{11}$$

The displacement field and radial stress generated by the scattering wave $W^{(S2)}$ occurred by T_D in area Ⅱ in the complex plane z_1 is:

$$W^{(S2)}_{(z_1,\bar{z}_1)}=\sum_{n=-\infty}^{n=+\infty}B_nH_n^{(1)}\left(k_2|z_1|\right)\left(z_1/|z_1|\right)^n \tag{12}$$

$$\tau^{(S2)}_{z\rho,(z_1,\bar{z}_1)}=0.5k_2G_2\sum_{n=-\infty}^{n=+\infty}B_n\left[H_{n-1}^{(1)}\left(k_2|z_1|\right)-H_{n+1}^{(1)}\left(k_2|z_1|\right)\right]\left(z_1/|z_1|\right)^n \tag{13}$$

In the complex plane z_1, the formulas (12) ~ (13) could be shown as:

$$W^{(S2)}_{(z_2,\bar{z}_2)}=\sum_{n=-\infty}^{n=+\infty}B_nH_n^{(1)}\left[k_2|z_2+i(R_D+h_2)|\right]\left\{\left[z_2+i(R_D+h_2)\right]/|z_2+i(R_D+h_2)|\right\}^n \tag{14}$$

$$\tau^{(S2)}_{z\rho,(z_2,\bar{z}_2)}=0.5k_2G_2\sum_{n=-\infty}^{n=+\infty}B_n\left\{\begin{array}{l}H_{n-1}^{(1)}\left[k_2|z_2+i(R_D+h_2)|\right]\left\{\left[z_2+i(R_D+h_2)\right]/|z_2+i(R_D+h_2)|\right\}^{n-1}\left(z_2/|z_2|\right)\\ -H_{n+1}^{(1)}\left[k_2|z_2+i(R_D+h_2)|\right]\left\{\left[z_2+i(R_D+h_2)\right]/|z_2+i(R_D+h_2)|\right\}^{n+1}\left(\bar{z}_2/|z_2|\right)\end{array}\right\} \tag{15}$$

After conformal mapping, the formulas (14) ~ (15) are changed to:

$$W^{(S2)}_{(\eta,\bar{\eta})}=\sum_{n=-\infty}^{n=+\infty}B_nH_n^{(1)}\left[k_2|f(\eta)+i(R_D+h_2)|\right]\left\{\left[f(\eta)+i(R_D+h_2)\right]/|f(\eta)+i(R_D+h_2)|\right\}^n \tag{16}$$

$$\tau^{(S2)}_{z\rho,(z_2,\bar{z}_2)}=0.5k_2G_2\sum_{n=-\infty}^{n=+\infty}B_n\left\{\begin{array}{l}H_{n-1}^{(1)}\left[k_2|f(\eta)+i(R_D+h_2)|\right]\left\{\frac{\left[f(\eta)+i(R_D+h_2)\right]}{|f(\eta)+i(R_D+h_2)|}\right\}^{n-1}\left\{\frac{\eta f'(\eta)}{|\eta f'(\eta)|}\right\}\\ -H_{n+1}^{(1)}\left[k_2|f(\eta)+i(R_D+h_2)|\right]\left\{\frac{\left[f(\eta)+i(R_D+h_2)\right]}{|f(\eta)+i(R_D+h_2)|}\right\}^{n+1}\left\{\frac{\bar{\eta}f'(\bar{\eta})}{|\eta f'(\eta)|}\right\}\end{array}\right\} \tag{17}$$

In the complex plane z_2, the displacement field and radial stress generated by the scattering wave $W^{(S3)}$ occurred by T_E in the area Ⅱ could be described as

$$W^{(S3)}_{(z_2,\bar{z}_2)}=\sum_{n=-\infty}^{n=+\infty}C_nH_n^{(1)}\left(k_2|z_2|\right)\left(z_2/|z_2|\right)^n \tag{18}$$

$$\tau^{(S3)}_{z\rho,(z_2,\bar{z}_2)}=0.5k_2G_2\sum_{n=-\infty}^{n=+\infty}C_n\left[H_{n-1}^{(1)}\left(k_2|z_2|\right)-H_{n+1}^{(1)}\left(k_2|z_2|\right)\right]\left(z_2/|z_2|\right)^n \tag{19}$$

In the complex plane z_1, the formulas (18) ~ (19) could be shown as:

$$W_{(z_1,\bar{z}_1)}^{(S3)}=\sum_{n=-\infty}^{n=+\infty}C_nH_n^{(1)}\left[k_2|z_1-i(R_D+h_2)|\right]\left\{\left[z_1-i(R_D+h_2)\right]/|z_1-i(R_D+h_2)|\right\}^n \tag{20}$$

$$\tau_{z\rho,(z_1,\bar{z}_1)}^{(S3)}=0.5k_2G_2\sum_{n=-\infty}^{n=+\infty}C_n\begin{Bmatrix}H_{n-1}^{(1)}\left[k_2|z_1-i(R_D+h_2)|\right]\left\{\left[z_1-i(R_D+h_2)\right]/|z_1-i(R_D+h_2)|\right\}^{n-1}\left(z_1/|z_1|\right)\\-H_{n+1}^{(1)}\left[k_2|z_1-i(R_D+h_2)|\right]\left\{\left[z_1-i(R_D+h_2)\right]/|z_1-i(R_D+h_2)|\right\}^{n+1}\left(z_1/|z_1|\right)\end{Bmatrix} \tag{21}$$

After conformal mapping, the formulas (13) ~ (15) are changed to:

$$W_{(\eta,\bar{\eta})}^{(S3)}=\sum_{n=-\infty}^{n=+\infty}C_nH_n^{(1)}\left[k_2|f(\eta)|\right]\left[f(\eta)/|f(\eta)|\right]^n \tag{22}$$

$$\tau_{zr,(\eta,\bar{\eta})}^{(S3)}=0.5k_2G_2\sum_{n=-\infty}^{n=+\infty}C_n\begin{Bmatrix}H_{n-1}^{(1)}\left[k_2|f(\eta)|\right]\left[f(\eta)/|f(\eta)|\right]^{n-1}\left[\eta f'(\eta)/|\eta f'(\eta)|\right]\\-H_{n+1}^{(1)}\left[k_2|f(\eta)|\right]\left[f(\eta)/|f(\eta)|\right]^{n+1}\left[\bar{\eta}f'(\bar{\eta})/|\eta f'(\eta)|\right]\end{Bmatrix} \tag{23}$$

The displacement field and radial stress generated by the scattering wave $W^{(S4)}$ occurred by T_U in areaIIin the complex plane z_1 is:

$$W_{(z_1,\bar{z}_1)}^{(S4)}=\sum_{n=-\infty}^{n=+\infty}D_nH_n^{(2)}\left(k_2|z_1|\right)\left(z_1/|z_1|\right)^n \tag{24}$$

$$\tau_{z\rho,(z_1,\bar{z}_1)}^{(S4)}=0.5k_2G_2\sum_{n=-\infty}^{n=+\infty}D_n\left[H_{n-1}^{(2)}\left(k_2|z_1|\right)-H_{n+1}^{(2)}\left(k_2|z_1|\right)\right]\left(z_1/|z_1|\right)^n \tag{25}$$

In the complex plane z_2, the formulas (24) ~ (25) could be shown as:

$$W_{(z_2,\bar{z}_2)}^{(S4)}=\sum_{n=-\infty}^{n=+\infty}D_nH_n^{(2)}\left[k_2|z_2+i(R_D+h_2)|\right]\left\{\left[z_2+i(R_D+h_2)\right]/|z_2+i(R_D+h_2)|\right\}^n \tag{26}$$

$$\tau_{z\rho,(z_2,\bar{z}_2)}^{(S4)}=0.5k_2G_2\sum_{n=-\infty}^{n=+\infty}D_n\begin{Bmatrix}H_{n-1}^{(2)}\left[k_2|z_2+i(R_D+h_2)|\right]\left\{\left[z_2+i(R_D+h_2)\right]/|z_2+i(R_D+h_2)|\right\}^{n-1}\left(z_2/|z_2|\right)\\-H_{n+1}^{(2)}\left[k_2|z_2+i(R_D+h_2)|\right]\left\{\left[z_2+i(R_D+h_2)\right]/|z_2+i(R_D+h_2)|\right\}^{n+1}\left(\bar{z}_2/|z_2|\right)\end{Bmatrix} \tag{27}$$

After conformal mapping, the formulas (26) ~ (27) are changed to:

$$W_{(\eta,\bar{\eta})}^{(S4)}=\sum_{n=-\infty}^{n=+\infty}D_nH_n^{(2)}\left[k_2|f(\eta)+i(R_D+h_2)|\right]\left\{\left[f(\eta)+i(R_D+h_2)\right]/|f(\eta)+i(R_D+h_2)|\right\}^n \tag{28}$$

$$\tau_{zr,(\eta,\bar{\eta})}^{(S4)}=0.5k_2G_2\sum_{n=-\infty}^{n=+\infty}D_n\begin{Bmatrix}H_{n-1}^{(2)}\left[k_2|f(\eta)+i(R_D+h_2)|\right]\left[\dfrac{f(\eta)+i(R_D+h_2)}{|f(\eta)+i(R_D+h_2)|}\right]^{n-1}\dfrac{\eta f'(\eta)}{|\eta f'(\eta)|}\\-H_{n+1}^{(2)}\left[k_2|f(\eta)+i(R_D+h_2)|\right]\left[\dfrac{f(\eta)+i(R_D+h_2)}{|f(\eta)+i(R_D+h_2)|}\right]^{n+1}\dfrac{\bar{\eta}f'(\bar{\eta})}{|\eta f'(\eta)|}\end{Bmatrix} \tag{29}$$

2.3. Equations set

Based on the boundary and junction condition, that the radial stress of T_U and TE is free and the displacement and radial stress of T_D are continuous, the set of equations could be expressed as:

$$\begin{cases}(a)\,T_D\left(|z_1|=R_D\right):W_{(z_1,\bar{z}_1)}^{(I)}+W_{(z_1,\bar{z}_1)}^{(S1)}=W_{(z_1,\bar{z}_1)}^{(S2)}+W_{(z_1,\bar{z}_1)}^{(S3)}+W_{(z_1,\bar{z}_1)}^{(S4)}\\(b)\,T_D\left(|z_1|=R_D\right):\tau_{z\rho,(z_1,\bar{z}_1)}^{(I)}+\tau_{z\rho,(z_1,\bar{z}_1)}^{(S1)}=\tau_{z\rho,(z_1,\bar{z}_1)}^{(S2)}+\tau_{z\rho,(z_1,\bar{z}_1)}^{(S3)}+\tau_{z\rho,(z_1,\bar{z}_1)}^{(S4)}\\(c)\,T_E\left(|\eta|=1\right):\tau_{zr,(\eta,\bar{\eta})}^{(S2)}+\tau_{zr,(\eta,\bar{\eta})}^{(S3)}+\tau_{zr,(\eta,\bar{\eta})}^{(S4)}=0\\(d)\,T_U\left(|z_1|=R_U\right):\tau_{z\rho,(z_1,\bar{z}_1)}^{(S2)}+\tau_{z\rho,(z_1,\bar{z}_1)}^{(S3)}+\tau_{z\rho,(z_1,\bar{z}_1)}^{(S4)}=0\end{cases} \tag{30}$$

Bring formulas (8) ~ (29) to formula (30), and take the known quantity to the right hand side of the equals sign and the unknown quantity to the left hand side, the equation (30) is changed as:

$$\sum_{n=-\infty}^{n=+\infty}\begin{bmatrix}\zeta_n^{(11)} & \zeta_n^{(12)} & \zeta_n^{(13)} & \zeta_n^{(14)}\\ \zeta_n^{(21)} & \zeta_n^{(22)} & \zeta_n^{(23)} & \zeta_n^{(24)}\\ \zeta_n^{(31)} & \zeta_n^{(32)} & \zeta_n^{(33)} & \zeta_n^{(34)}\\ \zeta_n^{(41)} & \zeta_n^{(42)} & \zeta_n^{(43)} & \zeta_n^{(44)}\end{bmatrix}\begin{bmatrix}A_n\\ B_n\\ C_n\\ D_n\end{bmatrix}=\begin{bmatrix}\delta_1\\ \delta_2\\ \delta_3\\ \delta_4\end{bmatrix} \tag{31}$$

Multiply both sides by exp(-imφ), and integrate them in (-π, π) respective, the coefficient An~Dn could be get, take them to the formulas and intercept limited items, all the unknown quantities will be found out.

2.4. The ground movement amplification coefficient (W)*

Define W* as the ground movement amplification coefficient:

$$W^* = \left|\left(W^{(S2)}_{(z_1,\bar{z}_1)} + W^{(S3)}_{(z_1,\bar{z}_1)} + W^{(S4)}_{(z_1,\bar{z}_1)}\right) \Big/ W_0\right|_{|z_1|=R_U} \tag{32}$$

3. Numerical Example

In this numerical example, the long axis of ellipse is assumed as 1, and the short axis is 0.9, that is to say a=1 and b=0.9. Define the parameters combination G*=G2/G1, k*=k2/k1. If k*<1 means the region I is harder than region II.

Figure 2 shows the ground surface displacement amplification coefficient W* with x1/r when the incident angle is 90o, the circular hole is in the middle of the layer, the thickness of the layer is 3 times of the long axis of the ellipse hole, G* is 1, the incident wave is in different frequency. Figure 2(a) shows that when the incident wave is in very low frequency, the curve shapes are almost the same, and with the increase of k*, the W* gradually decrease. Figure 2(b) and figure 2(c) are similar to figure 2(a), but the graphic shapes change to curve when the parameter k* increase. It is observed that the more difference of the wave numbers between the half space and the covering layer, the less of W* and the vibrations of W* are getting worse. It is also observed that with the incident wave number increase, the W* decrease gradually.

Figure 3 shows the change of W* with the location of the circular cavity. If the layer is softer than the half space, the larger of h1, the larger of W*. If the half space is softer than the layer, the W* is very complex. Generally speaking, when the ellipse cavity is in the middle of the layer, the W* is minimum, if the layer is harder than the half space.

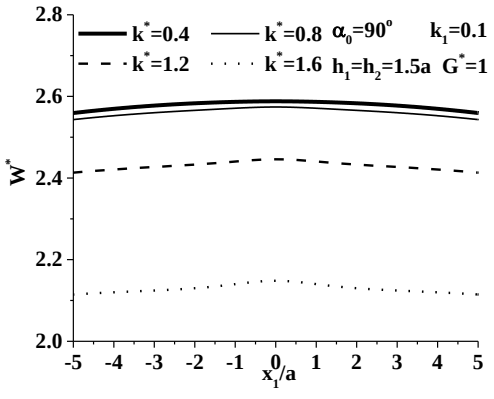

(a) k_1=0.1

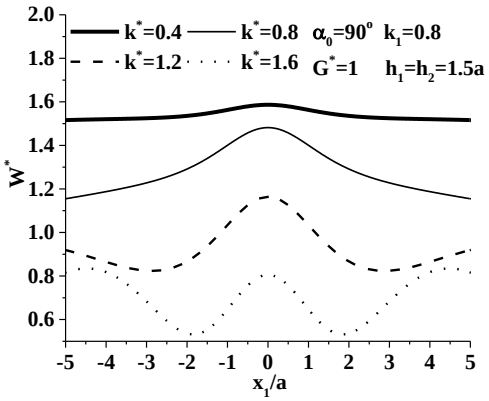

(b) k_1=0.8

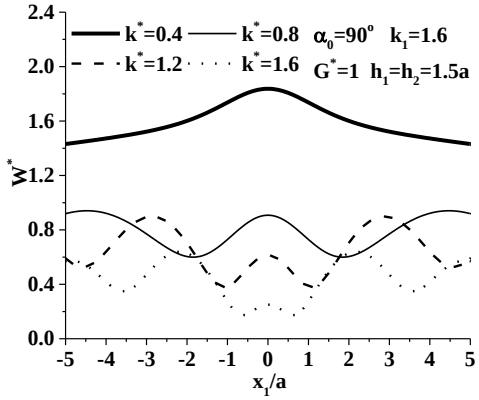

(c) k_1=1.6

Figure 2 The ground movement amplification coefficient W* of k* with X1/a (G*=1, h1= h2=1.5a, α0=90o)

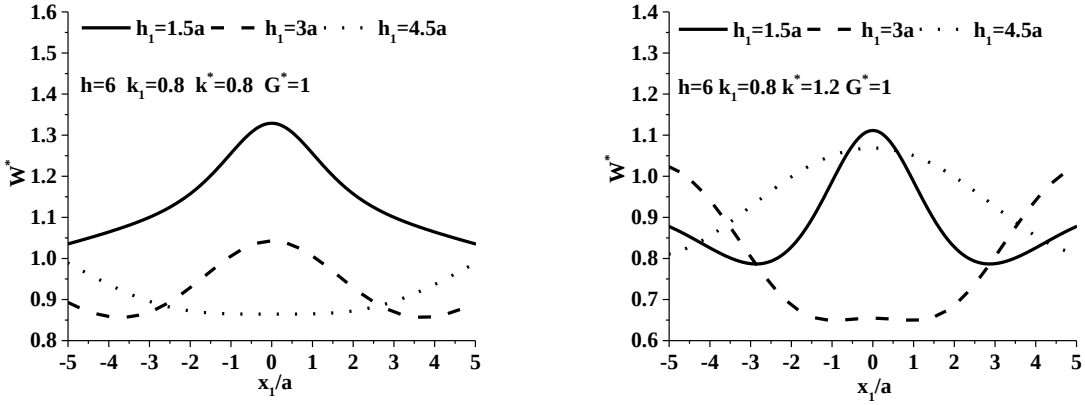

(a) k^*=0.8 (b) k^*=1.2

Figure 3 The ground movement amplification coefficient W* of h_1 with X_1/a (k_1=0.8, G^*=1, h=6, $\alpha_0=90^o$)

4. Conclusion

Based on the great arc hypothesis method and the conformal mapping transformation method, the ground movement of layer half space with a ellipse hole was studied. When the wave number of half space k1 is confirmed, the softer of the covering layer, the large of the ground movement. When the thickness of the covering layer is confirmed, the surface motion amplitude is decreased with the increasement of the distance between the ground surface and the center of the ellipse hole.

References

[1] Pao Y H, Mow C C. Diffraction of elastic waves and dynamic stress concentrations[M]. Crane, Russak, 1973: 193-198.
[2] Yuan X, Liao Z-P. Surface motion of a cylindrical hill of circular—arc cross-section for incident plane SH waves[J]. Soil Dynamics and Earthquake Engineering, 1996, 15(3): 189-199.
[3] Yuan X, Men F L. Scattering of plane sh waves by a semi‐cylindrical hill[J]. Earthquake Engineering & Structural Dynamics, 2010, 21(12): 1091-1098.
[4] Ning Z, Yufeng G, Jie Y, et al. An analytical solution to the scattering of cylindrical SH waves by a partially filled semi-circular alluvial valley: near-source site effects[J]. Earthquake

Engineering and Engineering Vibration, 2015, (02): 189-201.
[5] Liu D, Gai B, Tao G. Applications of the method of complex function to dynamic stress concentration. Wave Motion 4:293-304[J]. Wave Motion, 1982, 4(3): 293–304.
[6] Hui Q I, Shi Y, Chen D N. Scattering of SH-wave in a layered half-space with a subsurface circular cavity[J]. Journal of Harbin Engineering University, 2009, 30(5): 513-517.
[7] Chen D, Hui Q I. Dynamic analysis for circular cavity and inclusion impacted by SH-wave in a layered half-space[J]. Journal of Harbin Engineering University, 2014, 35(2): 171-176.
[8] Zhao Y, Qi H, Ding X, et al. The ground surface displacement of shallow buried circular cavity in a soft layered half-space impacted by SH wave[C]. International Conference on Energy, Environment and Materials Science, EEMS 2015, August 25, 2015 - August 26, 2015, 2016: 253-257.
[9] Ding X, Qi H, Zhao Y, et al. Ground motion of half space with ellipse inclusion and interfacial crack for SH waves[C]. International Conference on Energy, Environment and Materials Science, EEMS 2015, August 25, 2015 - August 26, 2015, 2016: 469-473.